https://doi.org/10.1142/9789811278952_0006

Chapter 6

Superconducting Magnet Technology for the IR Upgrade

E. Todesco[a], G. Ambrosio[b], P. Ferracin[c], G. L. Sabbi[d], T. Nakamoto[e], M. Sugano[e], R. Van Weelderen[a], P. Fabbricatore[f], S. Farinon[f], F. Toral[g], M. Sorbi[h], M. Statera[h], Q. Xu[i], J. M. Rifflet[j] and H. Felice[j]

[a]*CERN, TE Department, Genève 23, CH-1211, Switzerland*
[b]*FNAL, Batavia, IL, USA*
[c]*LBNL, Berkeley, CA, USA*
[d]*SLAC, Menlo Park, CA, USA*
[e]*KEK, Tsukuba, Japan*
[f]*INFN Genoa, Italy*
[g]*CIEMAT, Madrid, Spain*
[h]*INFN LASA, Milano, Italy*
[i]*IHEP, Beijing, China*
[j]*CEA Saclay, France*

In this section we present the magnet technology for the High Luminosity LHC. After a short review of the project targets and constraints, we discuss the main guidelines used to determine the technology, the field/gradients, the operational margins, and the choice of the current density for each type of magnet. Then we discuss the peculiar aspects of the design of each class of magnet, with special emphasis on the triplet.

1. Targets

The HL-LHC aims at gathering 3000 fb^{-1} over ten years. As discussed in the previous section, this ambitious target can be obtained by operating with a peak luminosity levelled at 5×10^{34} cm^{-2} s^{-1}. The plan is to obtain it through

higher intensity/lower emittance and a larger focusing on the Interaction Point (IP). This second part is given by the magnetic lattice; the target is to be able to reduce the beam size in the IP by a factor two, and therefore, at zero order approximation, one has double the size of the quadrupoles aperture in front of the IP (triplet).

Some of the previous proposals, done during the LHC luminosity upgrade studies [1,2,3], aimed at a reduction of the beam size of 30%, increasing the triplet aperture 30% (see Figure 1 for an historical view of the aperture proposed for the triplet). The HL-LHC target of reducing the beam size in the IP by a factor of two was based on theoretical studies (see for instance [4]), and was enabled by advances in magnet technology, i.e., test results from model quadrupoles of progressively larger aperture (Figure 1).

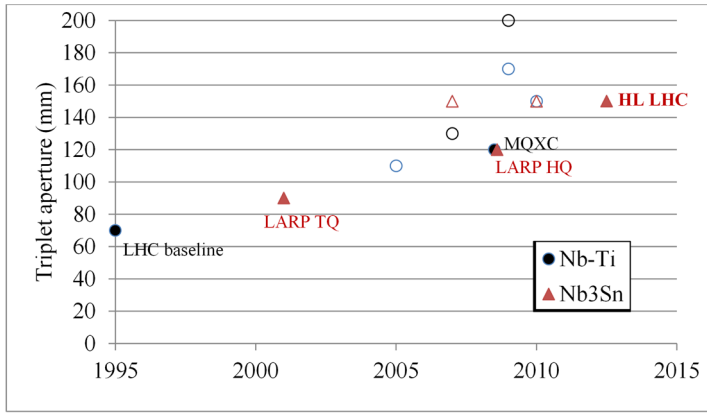

Fig. 1. Proposed aperture for the inner triplet versus time: triangle (Nb_3Sn), circles (Nb-Ti), built hardware in full markers, and proposal in empty markers.

A critical design parameter for a superconducting quadrupole is the peak field in the coil, which is a function of the aperture times the gradient. For Nb-Ti dipole coils the peak field limit in operational conditions is ~8-9 T [5], whereas for Nb_3Sn this limit is ~15 T. One can prove that for quadrupoles Nb_3Sn can give 50% more gradient w.r.t. Nb-Ti for the same aperture [6] (see Figure 2): this allows for shorter magnets compared to Nb-Ti. As explained in the previous chaper, a compact triplet means not only more space for other components, in a critical region of the tunnel, but also additional performance: a shorter triplet means that the beam size has less longitudinal

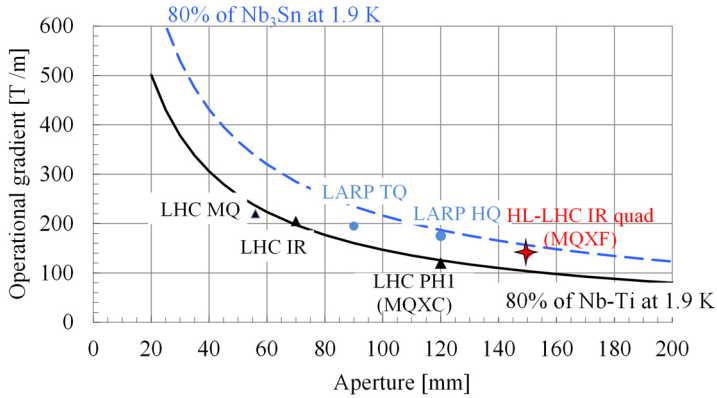

Fig. 2. Operational gradient versus aperture in Nb-Ti and Nb_3Sn quadrupoles.

space to grow, and therefore for the same aperture one can squeeze more the beam in the IP. Moreover, a shorter triplet allows reducing the number of long range beam-beam interactions and to reduce chromatic aberrations. So, Nb_3Sn is the enabling technology to reach the ambitious target of the HL-LHC project. Finally, another fundamental aspect is to use the additional aperture to house a massive shielding to reduce the heat load and the radiation damage, as discussed in the next section.

2. Constraints

2.1. *Radiation damage and heat load*

The design of the final focus system of the upgraded LHC needs to account for the special conditions related to its proximity to the interaction points. The first important constraint for the magnetic system is the radiation damage, which is proportional to the integrated luminosity. Some essential components employed for magnet fabrication (epoxy resins) undergo severe degradation at 50-100 MGy. Therefore, one needs to set a safe dose limit of 10-20 MGy or switch to the complexity related to radiation resistant materials, as used for nuclear fusion, which can operate in the range of 100 MGy and more. For the HL-LHC we set a target for radiation damage at ~30 MGy.

The second relevant constraint for the magnetic system is the heat deposition on the coil, which is proportional to the peak luminosity. In the

stationary regime of continuous heat deposition, it induces a temperature gradient between the helium bath (T_{bath}=1.9 K) and the temperature of the coil T_{coil}=(1.9+ΔT). In the LHC triplet, the limit to the heat load is given by the requirement of having superfluid helium in the coil, at a temperature of 1.9 K giving a ΔT<0.27 K margin to the lambda point [7]. The actual design limit is set to one third of the theoretical ΔT in order to account for uncertainties in the thermal analysis or variations in the heat load and cooling conditions. For the present inner triplet quadrupoles built with Nb-Ti conductor, this corresponds to a power deposition limit of 4 mW/cm^3, with a safety factor 3. For Nb_3Sn, with the same safety factor, one can withstand 12 mW/cm^3 [8].

Simulations of energy deposition in the HL-LHC show that without any shielding one has about 200 MGy peak dose and a peak heat load of 20 mW/cm^3. This regime is not acceptable for both aspects. The peak is localized in the horizontal and vertical planes. Shielding is very effective: with a 6-mm-thick tungsten shielding, one can bring these values down by a factor five, i.e. to 40 MGy and 4 mW/cm^3 [9].

Using an additional shielding in the quadrupole Q1 close to the IP (see Figure 3), where the aperture requirement is smaller due to a smaller size of the beam, one can further reduce these values by a factor two. Therefore,

Fig. 3. Prototype of beam screen and tungsten shielding in Q1.

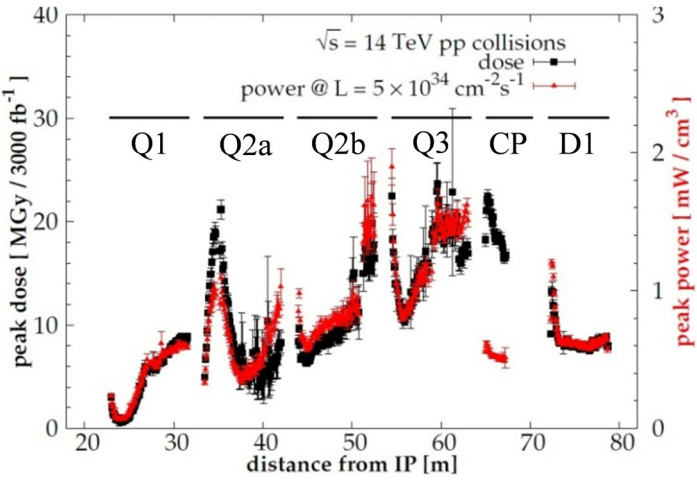

Fig. 4. Heat deposition in the coil (left scale), and radiation damage (right scale) for the 150 mm aperture triplet.

one ends up with a radiation dose similar to what is expected for the LHC, having a factor ten less integrated luminosity, (20-25 MGy) and an even lower heat load (2 mW/cm^3), see Figure 4.

The absorbers installed in the magnet bore address two of the most significant challenges of the LHC luminosity upgrade, namely the radiation damage and the heat load. To maintain the required space for the beam the final aperture of the quadrupoles has been fixed to 150 mm, i.e. slightly more than twice the present triplet.

Two additional requirements point in the direction of a thick shielding as the only viable choice for the project. The total heat load on the triplet and separation dipole is 1.5 kW over 55 m, i.e. 30 W/m. The massive shielding allows to intercept about 800 W in the beam screen+shielding and remove it at intermediate temperature with higher efficiency. The remaining 700 W load needs to be removed from the cold mass at 1.9 K. This requires two heat exchangers of 70 mm diameter, barely fitting into the magnet cross-section. A larger heat load would require larger heat exchangers, and larger magnet diameter, which is already at the limit of the constraints imposed by the tunnel diameter.

The second aspect is the degradation of copper Residual Resistivity Ratio (RRR) due to the radiation dose. This parameter is defined as the ratio between

the resistivity at room temperature and at 1.9 K, related to the purity of copper, RRR must be >150 to guarantee the conductor stability and a proper protection in case of quench. Recent studies pointed out that with 200 MGy the RRR is reduced by one order of magnitude [10]. Therefore, a dose of 200 MGy would also endanger the magnet operation and its protection. This degradation is partially wiped out by a warm-up to room temperature, so one could have problems in case of very long runs without warm-up. However, with the 6-mm-thick shielding, the copper RRR degradation becomes negligible.

2.2. *Field quality*

The beta functions in the triplet become very large during the operation with collisions for physics, reaching peak values of ~20 km, i.e. five times larger than the nominal LHC values. In these conditions, the beams become very sensitive to magnetic field errors: for this reason, the field quality constraints are very tight. On the other hand, at injection the interaction region gives a small contribution to the total budget of field imperfection of the accelerator and therefore the field quality targets can be significantly relaxed. The field quality optimization should therefore concentrate on high field conditions. A large set of corrector magnets (up to order 6) is foreseen in the layout to be able to correct field errors and/or add nonlinearities to counter beam instabilities; in fact, since the beam size is very large in the correctors, they are very effective to correct any nonlinear unwanted component of the whole LHC.

2.3. *Fringe field and magnet size*

We roughly double the magnet apertures w.r.t. the LHC baseline, but the size of the cold mass is limited by the maximum cryostat size. In the LHC we have a cryostat with a 980 mm diameter that is not far from the limit imposed by the tunnel transverse size. In HL-LHC, the cold mass size is increased from 570 to 630 mm to partly compensate for the aperture, with a weight increase of less than 20%. Larger cold mass diameters would have been difficult since some clearance is needed between the cryostat and the magnet.

In these conditions it is unavoidable to have a large magnetic field outside the cryostat: the transverse fringe field reaches ~50 mT on the cryostat surface.

There is no specification of the allowed field in the LHC tunnel; this value depends on the specific instrumentation in situ (vacuum valves, beam position monitors, beam loss monitors, quench protection equipment …) and in some cases one can envisage a displacement or shielding of the instrument (which is less invasive than shielding the magnet. A target of 50 mT maximum field on the cryostat is considered to be compatible with HL-LHC operation). An alternative solution is an active magnetic shielding, but at the price of an increased complexity of interconnections and number of components.

3. Main Design Choices

3.1. *Foreword: loadline, critical surface, and margin*

A superconducting magnet has most of the field produced by transport current, plus a second order contribution given by the iron magnetization: therefore, in a first approximation the field is proportional to the current density in the coil: the relation peak field in the coil B_p versus current density j is called the loadline.

A superconducting coil can tolerate up to a given combination of field, current density and operational temperature: this is a property of the superconductor called the critical surface. Materials that can tolerate larger values of field and current density have a better performance, allowing to reach larger fields or to make more compact coils. When the loadline crosses the critical surface, one has the maximum theoretical reachable field. It is called short sample limit since the critical surface is usually measured for a short sample of conductor.

A critical choice for magnet design is the width of its winding. The peak field is proportional to the current density and to the width of the coil, so with large coil widths, the loadline in the *B-j* graph has a lower slope and one can reach higher fields using lower current densities (see Figure 5). However, a magnet with larger coil is less effective, less compact, and therefore requires more superconductors. With larger and larger coils an asymptotic field is reached, the gain in the short sample limit becoming more and more marginal: one needs to find the optimal coil width. The history of the accelerator magnets shows a progressive increase of coil widths to achieve higher fields [11].

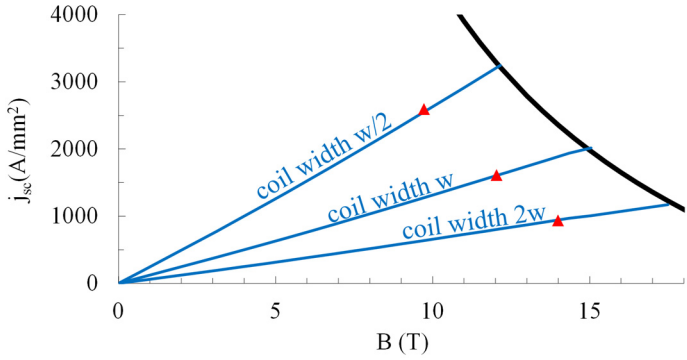

Fig. 5. Critical current versus field for Nb_3Sn at 1.9 K, and loadlines for a coil with width w, w/2 and 2w; red dots indicate operational points with 20% margin.

There are two more aspects that add to what may seem a pure cost and size problem (see also [12,13]): firstly, larger current densities imply larger mechanical stress induced by the electromagnetic. This aspect is particularly critical for HL-LHC since accumulation of azimuthal stress is also proportional to the magnet aperture, and therefore large values are reached even for intermediate fields of the order of 6 T. The second aspect is protection: in case of a transition from the superconductive to the resistive state, the energy of the magnetic field has to be dissipated in the coil. A too large energy density brings the coil to an unsafe temperature (usually considered to be above 350 K) or temperature gradient that damages it. Both stress and protection aspects point to avoid current densities in the coil (including insulation, but not wedges) well above 600 A/mm^2.

Finally, the design needs to account for production and operation margins. Main magnets in particle accelerators usually operate at 50%-80% of the short sample limit, and correctors around 50%, according to the magnet type and technology. Since the operational targets are usually established before magnet prototyping and production, their selection needs to take into account cost, risk and performance considerations. In the following, we will carry out the main choices for the HL-LHC magnets: technology, coil width and operational margin. A first baseline was developed in 2013 [12] and went through few minor iterations; the final layout is given in [13]. A list of the parameters is given in Table 1.

Table 1. Parameters of HL-LHC main magnets and dipole correctors

		MQXFA/B	MCBXFA/B	D1	D2	MCBRD
Magnet Aperture	(mm)	150	150	150	105	105
Integrated Field	T (m)	-	2.5/4.5	35	35	5
Integrated Gradient	(T)	556.9/948.1	-	-	-	-
Field	(T)	132.6	2.10/2.15	5.60	4.50	2.60
Mag. Length	(m)	4.20/7.15	2.10/1.20	6.26	7.78	1.92
N. Apertures		1	1	1	2	3
Material		Nb_3Sn	Nb-Ti	Nb-Ti	Nb-Ti	Nb-Ti
Strand Diameter	(mm)	0.850	0.480	0.825	0.825	0.825
Peak Field	(T)	11.4	4.13	6.58	5.26	2.94
Op. Temp.	(K)	1.9	1.9	1.9	1.9	1.9
Current	(A)	16230	1580-1400	12047	12328	392
J Overall	(A/mm^2)	462	306-270	449	478	368
Loadline Fraction		0.77	0.50	0.77	0.68	0.47
Stored Energy	(MJ)	4.91/8.37	0.77 – 0.239	2.13	2.26	0.143

3.2. *Technology, peak field, margin*

In a final focus system, performance is given by large aperture and short length in the region from the interaction point up to the separation dipole. This leads to use in the triplet the Nb_3Sn technology at 1.9 K, which allows doubling the aperture of the present Nb-Ti triplet with a moderate increase of the magnet length (see Figure 6). A point of equilibrium between maximization of performance and risking conditions associated with a low margin, was found at 78% on the loadline (see Figure 7).

For the separation/recombination dipole D1 (single aperture), which is presently a resistive magnet (see Figure 6), we opt for a superconducting magnet with 5.6 T operational field, based on Nb-Ti technology, with a 77% operational point on the loadline [14]. Here the initial value of 75% was changed to be able to fit the magnet in the vertical test station; the possibility of vertical testing represents a considerable risk reduction. This field value still fits to the field quality constraints imposing a limited variation of multipoles with nominal current to avoid reaching an uncontrolled situation.

With respect to the LHC, the reduction in the length of D1 in the upgraded IR more than compensates for the additional space needed by the triplet; in

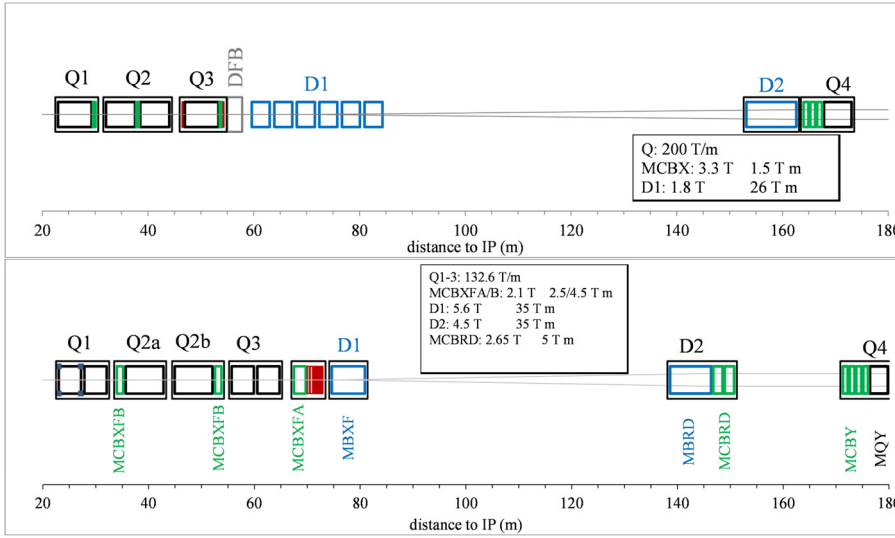

Fig. 6. Layout of the LHC (upper part) and of HL LHC (lower part) interaction region from first quadrupole (Q1) to separation dipole (D1).

fact, the end of D1 in the HL-LHC layout is 4 meters closer to the interaction point as compared to the LHC. The option of a Nb_3Sn magnet, considered in the past [15], has been discarded as the gain of a few meters (3 m, with an 11 T dipole) is not considered critical in this location and has no effect on performance.

The maximum field in the separation/recombination dipole D2 (double aperture) is also mainly determined by field quality constraints, i.e. avoiding a too large saturation in the iron. The issue is not the value itself, that can be corrected via the geometric contribution, but avoiding having a large derivative of b3 with respect to the operational field, that in the LHC should keep a flexibility in the range 6.5 to 7.5 TeV. For this reason we chose an operational field of 4.5 T based on the Nb-Ti technology, giving a more comfortable operational point at 68% on the loadline. The initial layout also considered a larger aperture Q4 [16], but this option was discarded in 2017, since the additional aperture was not considered to bring a significant performance improvement. However, one short model and two prototypes were built.

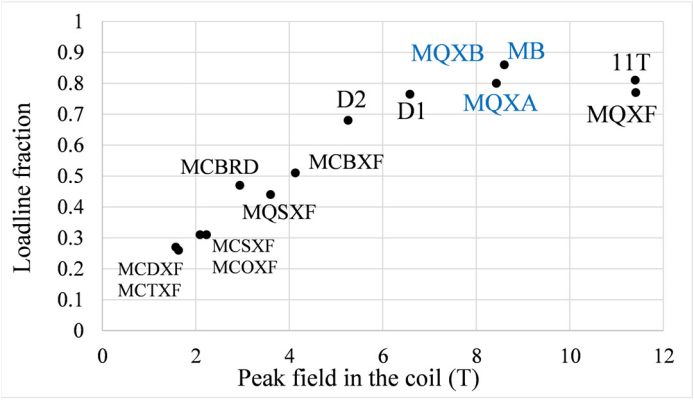

Fig. 7. Peak field in the coil versus loadline fraction of HL-LHC IR main magnets and correctors, 11 T. Blue points: LHC main dipole (MB) and LHC IR quadrupoles (MQXA and MQXB).

The correctors were selected to operate with lower loadline fraction (30% to 50%), as in most accelerators, as there is no need to increase the performance and the cost of additional margin is low compared to the case of the main magnets. The plot summarizing the peak field versus the loadline fraction is given in Figure 7, where the LHC magnets are also shown.

3.3. *Cable, coil width and stress*

The accumulation of stress in the midplane is proportional to the magnet aperture, to the field and to the current density. Therefore HL-LHC magnets naturally have much larger stress than the LHC magnets, just because of the larger aperture. Values approaching 200 MPa can damage insulation for Nb-Ti magnets or degrade conductor performances for the Nb_3Sn magnets. Therefore, one has to carefully check during the initial design phase that the field, aperture and current density values correspond to reasonable values of stress.

A way to reduce the stress enhancement is to use a larger coil width and reduce the current density, i.e. having a less effective magnet. In HL-LHC, we increased the coil width of the quadrupoles to a double layer of 18 mm width cable; moreover, both D1 and D2 were designed with coils reusing the Nb-Ti cable of the LHC, i.e. increasing the coil width by 50% with respect to the LHC superconducting D2 recombination dipoles, based on BNL RHIC dipole design [17] and 10-mm-width cable.

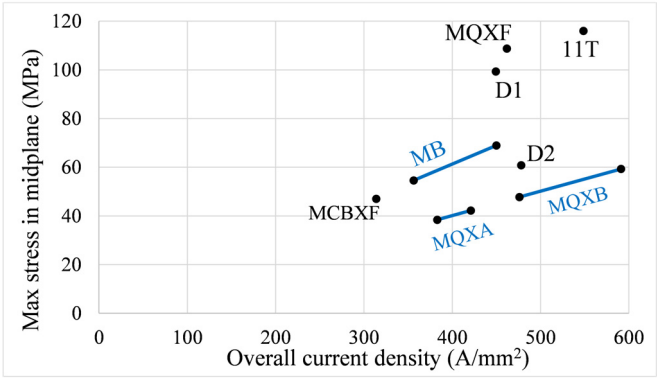

Fig. 8. Overall current density versus maximum midplane stress (in absence of structure and coil deformations) for HL-LHC IR main magnets, 11 T. Blue: LHC main dipole (MB) and LHC triplet (MQXA and MQXB), where two points are given (joint by a line to ease the readability) since the inner and outer layer have differen current densities.

The plot summarizing the overall current density versus the accumulated stress in the midplane is given in Figure 8: due to the large aperture, both the HL-LHC triplet MQXF and the separation dipole D1 have challenging values above 100 MPa, 50% to 100% larger than what present in the LHC dipoles.

3.4. *Cryostat and interconnections*

The maximum length of a cryostat that can be lowered in the tunnel is 15 m, corresponding to the main dipole case. Having quadrupoles with lengths ranging from 7 to 8 m, plus a series of orbit correctors, we are forced to have one cryostat per quadrupole (in LHC Q2a and Q2b share the same cryostat, see Figure 7). The US AUP project, in charge of Q1 and Q3, has opted for a solution based on having two 4.2-m-long quadrupoles closely connected to form one cryostat for the Q1 and Q3 units. This reduces the risk associated to the magnet length, even though it increases costs due to double number of coils and magnet assemblies, and requires doubling the manufacturing lines. The Q2 units are designed with one 7.15-m-long quadrupole magnet (magnetic length), making a further step in the length of Nb_3Sn coils towards the 15 m target needed for main dipoles of a future accelerator fully based on Nb_3Sn. The interconnections have been designed to minimize the distance between the magnets given the requirements for installation and interconnection.

3.5. *Cooling*

The cooling of the triplet is provided through heat exchangers. Since the total load on the cold mass is about 15 W/m, one has to use two heat exchangers of 70 mm diameter. The alternative options of one heat exchanger of 110 mm diameter would simplify the interconnections but is not viable since it is not compatible with the magnet mechanical structure. The ideal position for a hole in the yoke of a quadrupole is at 45°, i.e. in the low field region and where less material is needed for structural reasons. A 70 mm heat exchanger is large but still fits the cold mass iron yoke. The short orbit correctors have to share the heat exchanger, i.e. the hole must be in the same positions.

4. The Triplet Quadrupoles Q1-Q3

4.1. *Historical development*

The development of Nb_3Sn quadrupoles for the LHC luminosity upgrade was first initiated with the US conductor development program [18] and, in 2004, by the US LHC Accelerator Research Program (LARP), a collaboration of US National Laboratories and CERN [19]. At that time the target was to reach a β^* of 25 cm and a 30% increase of the aperture, from 70 to 90 mm was considered an adequate choice both in terms of machine requirements and technological challenges. After some preliminary tests using racetrack coils, the 1-m-long Technological Quadrupole (TQ) series were developed to address key manufacturing and design issues for $\cos 2\theta$ coils [19]. Two mechanical structures were tested, one based on stainless steel collars [19] and the other on Al shell pre-loaded using water-pressurized bladders and interference keys [19,20]. After testing several models, the bladder and key structure demonstrated a better capability of controlling stress and a better reproducibility of performance and was selected for the length scale-up from 1 m to 3.4 m (Long Quadrupole - LQ series, see Figure 9), with successful tests starting from 2009 [21].

Meanwhile, several studies were pointing at the possibility of using apertures larger than 90 mm to increase the upgrade performance [5]. In order to study the feasibility of larger apertures, and demonstrate the capability to incorporate field quality and alignment requirements, LARP started the

Fig. 9. LQ, the first 3.4-m-long Nb_3Sn magnet built by LARP collaboration.

development of the 120-mm-aperture High-field Quadrupole HQ in 2008 [22]. A successful HQ test at CERN in early 2012 supported the decision to further increase to 150 mm aperture for the triplet quadrupoles (MQXF) [12,23]. The most advanced solutions used in TQ, LQ and HQ are now being applied to the larger aperture quadrupole. So MQXF is essentially a scaling of the design of HQ. The guideline is to keep all features that have been shown to work in the LARP magnets.

4.2. *Strand and cable*

As the aperture in QXF is 25% larger than in HQ, a corresponding increase of the coil width is desirable. In order to minimize deviations from established LARP designs, a two-layer coil layout is maintained and the increase in coil width is obtained with an increase in cable width, requiring a larger strand and/or more strands per cable. The option of having one additional layer was excluded to avoid complexity in the coil fabrication. The number of strands is limited by cable mechanical instabilities which affect the winding process, and/or damage to the superconducting strands during the cabling operation. For MQXF, it has been decided to limit the number of strands to 40, which is also the upper limit of the CERN winding machine. TQ cable had 27 strands and 10 mm width, and HQ had 35 strands with 15 mm width. The number of strands and the cable width fixes the strand diameter to 0.85 mm. This is a

marginal increase compared to the HQ case, which had 0.8 mm. In all cases we tried to minimize the changes w.r.t. HQ magnets to rely on established design solutions and avoid significant delays to overcome new issues.

With respect to LARP workhorse, the RRP 0.7 mm strand with 54/61 layout, it was decided to use the latest developments used in HQ, i.e. finer filaments with 108/127 layout; the critical current density was reduced by about 10-20% with respect to the highest values reached for the RRP technology, and the specification was at 1280 A/mm2 at 4.22 K and 15 T.

The cable made use of a stainless steel core (25 μm thick) to increase the inter-strand resistance. Previous LARP quadrupoles, built without cored cables, showed a clear indication of a very low inter-strand resistance (of the order of 0.1-0.5 μΩ) [24], producing (i) a severe degradation of quench performance with increasing ramp rate, affecting the capability to perform a fast discharge without quench and (ii) a degradation of field quality, visible as non-allowed components with large dependence on ramp rate, and decay of several units even at high field, with times of the order of a few seconds (see Figure 10). The second short model HQ02, built with cored cable, proved to cure these issues with an increase of the effective inter-strand resistance by more than one order of magnitude (see Figure 11). Insulation is based on a braided fiberglass tape.

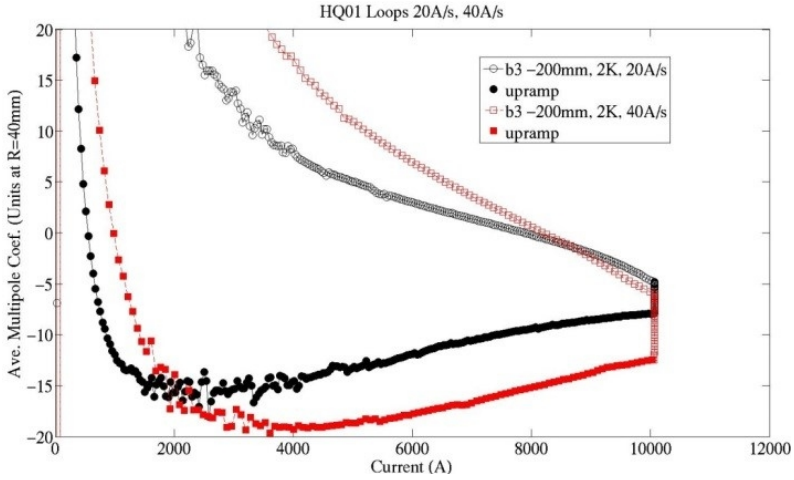

Fig. 10. Dependence of b_3 along the ramp for different ramp rates: case of cable without core (HQ01e).

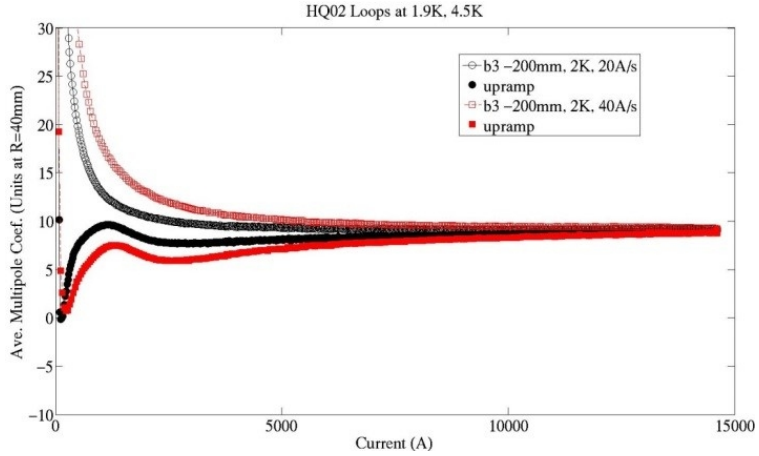

Fig. 11. Dependence of b_3 along the ramp for different ramp rates: case of cable with core (HQ02a).

4.3. *Coil*

The coil is a double layer, four block coil [23]. Two wedges provide the required flexibility to tune the field quality to optimal values. The basic layout of the conductor blocks (Figure 12) is similar to what has been used in HQ. In particular, similar pole angles are chosen for both layers. This approach has

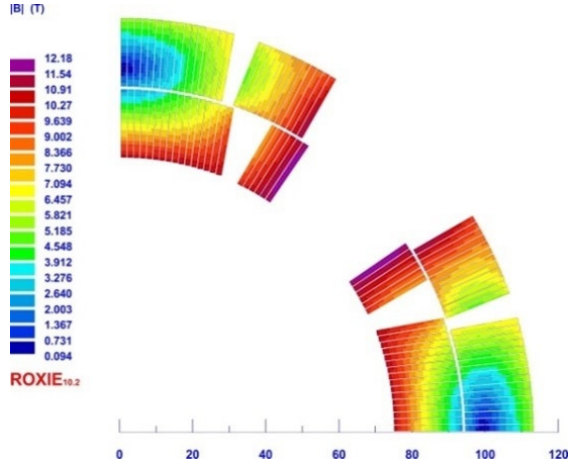

Fig. 12. MQXF coil cross-section (one quarter shown), and field in operational conditions.

been shown to minimize the peak coil stresses. In operational conditions the peak field in the coil is 11.4 T, corresponding to a ratio between peak field and gradient times aperture of about 1.15. The coil is reacted after winding, with a reaction cycle to form the Nb_3Sn superconductor followed by impregnation with CTD-101K. The 7.15-m-long coils of Q2 are shown in Figure 13.

Fig. 13. MQXF coils manufactured at CERN.

4.4. *Mechanical structure*

The magnetic forces are contained by an aluminium shell (see the MQXF cross-section in Figure 14 [23]). During the assembly at room temperature, a prestress of the order of 100 MPa is applied to the coil through the insertion of keys in the slots opened by bladders. During the cool down, the Al cylinder stress increases by an order of 30 additional MPa. This procedure has been used in several models, proving to be an efficient and accurate way to control the stress in the magnet, and allow to select a preload to fully or partially balance the electromagnetic forces. As the magnet is energized, the pre-load provided by the mechanical structure is replaced by the internal loads

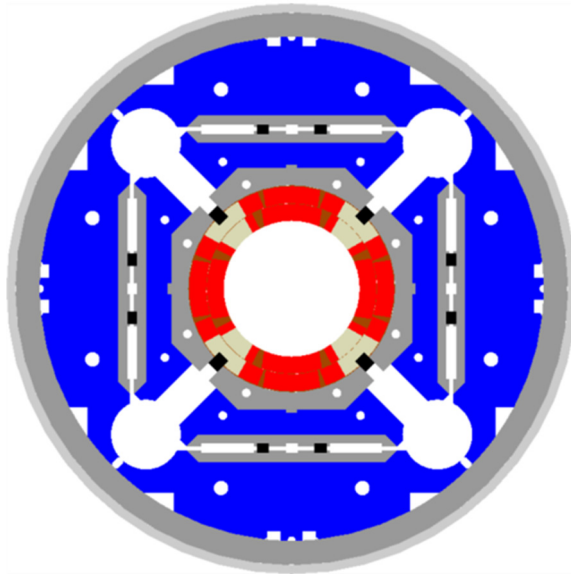

Fig. 14. MQXF cross-section.

generated inside the coils by the electro-magnetic forces. Full alignment is maintained at all steps of coil fabrication, magnet assembly and powering. An additional stainless-steel vessel is needed for He containment. The axial structure is based on stainless steel tie rods providing a preload on the magnet ends equivalent to the magnetic forces; this solution has been validated on the LARP magnets.

4.5. *Protection*

The inductance of the QXF magnets is 8-10 mH/m, the lowest value being at nominal current and the highest in the linear regime of non-saturated iron, i.e., at injection. The current is 17.5 kA, so a dump resistor is limited to 50 μΩ to avoid having voltages that exceed 900 V at the beginning of the current dump. In these conditions, a dump extracts a negligible fraction of the energy stored in the magnetic field, and as in the LHC dipoles, the only solution is to use the thermal inertia of the magnet coil to dissipate the energy of the magnetic field. A design constraint to remain below ~350 K in all points of the coils during a quench was adopted.

Both Nb-Ti and Nb_3Sn windings have a similar enthalpy from 2 K to 300 K of the order of 0.6 J/mm^3. So, the first physical quantity to check is the energy density, i.e., the stored energy divided by the volume of the coil. Note that due to the time scale involved in these phenomena (a fraction of second), the structure components as collars and yoke are too far from the coils to participate to share the burden of the heat dissipation – that's why we consider the energy density only over the coil volume. For typical Nb-Ti magnets this value is around 0.05 J/mm^3. In our case, as in many other Nb_3Sn magnets, we are at twice this value, so still well within the enthalpy limit but with half the margin.

The key point is to prevent excessive energy dissipation at the initial quench location, which can lead to coil damage due to high local temperature and stress, by ensuring rapid transition of the entire winding to the normal conducting state in the fastest possible time. This is done as in most accelerator magnets through quench heaters, i.e., strips of stainless steel which are powered as soon as the quench is detected, and whose heat is transferred via conduction to the coil, pushing it above the critical temperature.

A simple way to compare the protection challenge is to compute the time budget (time margin) for the protection system available to quench all magnet, setting 300 K as the maximum temperature reached by the coil [25]. An advantage of this quantity is that it depends only on the magnet design, and not on the quench features (high field or low field, propagation, etc.) and on the protection system. On the other hand, to make the estimate of the warmest point reached in the magnet (so-called hotspot temperature) one needs other hypothesis on the quench location, efficiency of heaters, propagation, etc.

The time margin is of the order of 100 ms for Nb-Ti magnets. In general, one needs a few ms to build enough resistance to have a measurable voltage (voltage thresholds are usually set at 100 mV). Then a validation window of 10 ms is used to avoid having false signals. Then the switch of the circuit disconnecting the power converter and dumping the current on the external resistor or on a diode is opened (2 ms). At the same time the heaters are fired. Typical times between the heater firing and the quench of the coil induced by the heaters is 10-20 ms (among the numerous literature, see [26] for an extensive overview). Therefore, 40 ms is a minimal value necessary to have a safe protection system: this is what is achieved in MQXF design. Note that for TQ and HQ magnet this margin is only 18 and 25 ms respectively.

The MQXF protection system relies on outer layer heaters. With respect to the LARP choices, the thickness of the insulation between the heater strip and the coil has been increased from 25 μm to 50 μm to reduce the risks related to insulation failures between the coil and the heaters. On the top of the outer layer quench heaters, two additional options were studied to add the redundancy and the robustness to failure scenarios that are required for operation. Note that the magnet has to be protected in case of two simultaneous failures.

The first redundant system that was explored is the use of inner layer quench heaters, having the interesting feature of directly quenching the inner layer, and not relying on the heat propagation from outer to inner layer. Inner layer quench heaters were intensively studied in LARP and in the initial part of MQXF program, showing a good efficiency in quenching the inner layer of the coil, but they were finally abandoned due to partial detachment of the heaters after successive quenches.

The second option was the use of a novel method [27] based on the injection of a fast pulse of currents in the opposite coils to provoke a quench thanks to the heat dissipation induced by the dI/dt (see Figure 15). This method, named CLIQ, proved to be extremely effective in quenching both layers and

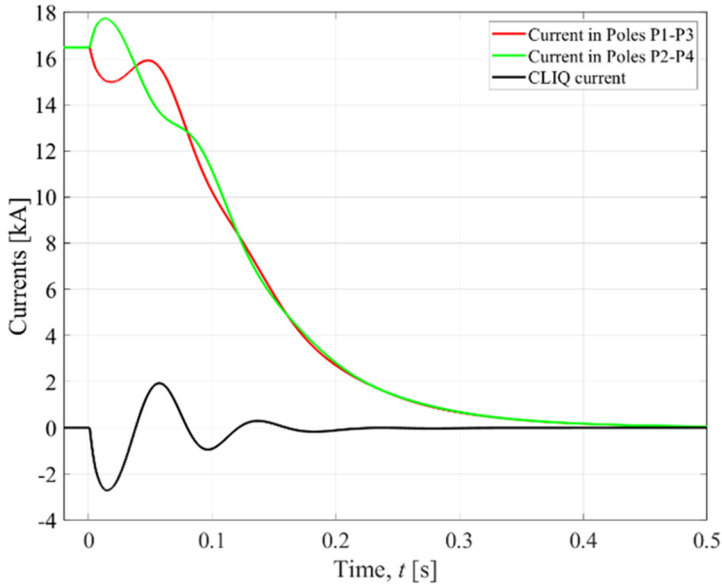

Fig. 15. Current decay during a quench induced via the CLIQ system.

is now part of the MQXF baseline, together with outer quench heaters [28]. In case of no failures, the use of CLIQ and outer layers quench heaters guarantees a hotspot temperature during quench below 300 K.

4.6. *Field quality and shimming*

When the beams are squeezed in the interaction point, the optical functions in the triplet are very large and the beam dynamics becomes very sensitive to any field imperfection in the triplet. Field quality of the triplet must satisfy tight constraints. The main challenges are (i) a reproducibility of the transfer function of less than one unit and (ii) control of the low order harmonics within few units. One the other hand, the nonlinearities coming from the large iron saturation (about 10%, as in HQ, see Figure 16) can be compensated through an adequate powering of the magnets, provided that the effect is reproducible. Results from the LARP program show that this level of reproducibility is obtained, and that there is a good understanding of the quadrupole main component behaviour as a function of the current and of the ramp direction.

The low order harmonics are related to the asymmetries of the components and of the assembly. Here, in the initial part of the production cases several units of non-allowed low-order harmonics (a_3, b_3, a_4, b_4) have been found. For

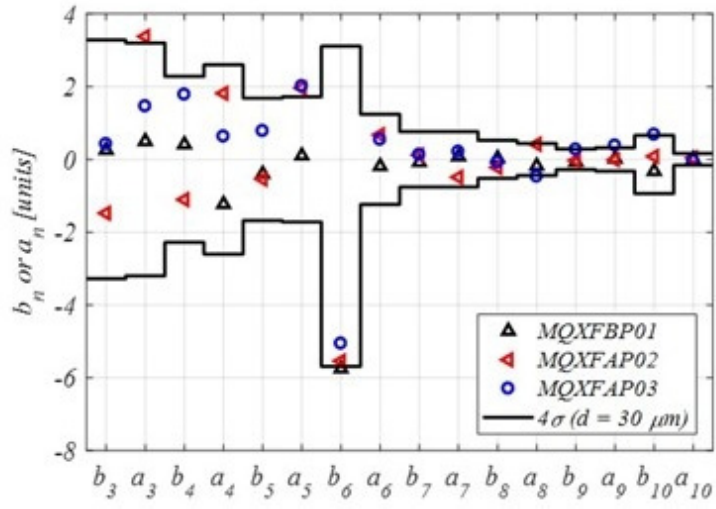

Fig. 16. Average field harmonics measured in three prototypes, and tolerance range.

this reason, a magnetic shimming [29] has been foreseen to compensate for a few large harmonics (typically two at the same time). The technique is based on inserting magnetic rods in holes in the collars and magnetic bars in the spaces used by the bladders. By placing magnetic shims in an asymmetric way, one can compensate up to several units of low order harmonics [30]. The more mature part of the production has shown a reduction of the non-allowed low order harmonics (see Figure 16), towards levels achieved in Nb-Ti collared magnets.

Usually, a lot of emphasis is put on the first allowed harmonics b_6. In fact, this harmonic is not the most critical for the beam, as it is a high order. Moreover, from the point of view of the magnet builder, it is pretty easy to control b_6 through the cross-section geometry. At injection one has about 20 units given by the magnetizations, which are within the beam dynamics targets.

4.7. *Present status*

The program includes six short models as a joint effort of CERN and AUP; for MQXFA, two prototypes, 5 pre-series and 16 series magnets are foreseen. For MQXFB, two prototypes and 10 series magnets. An overview on the performance of the short model and prototype magnet build so far goes behind the scope of this chapter, and we refer to [13] as the most recent reference available at the moment of writing.

5. Correctors

5.1. *Single-aperture nested orbit correctors*

The orbit correctors are needed to compensate for alignment errors of the triplet, to steer the closed orbit of the accelerator, and to open the crossing angle in the interaction point. For HL-LHC, two correctors providing 2.5 T m in each plane are needed close to each Q2, and one providing 4.5 T m between Q3 and D1 (see Figure 6). The aperture has to match the triplet and D1 aperture, i.e., 150 mm diameter. For comparison, in the LHC we have nested magnets providing 3 T in each plane, with 70 mm aperture. A nested configuration is needed to reduce the gap between the quadrupoles, which produces an increase of the beta functions and therefore of the beam size in the

triplet, requiring a larger aperture. The main challenge of the nested magnet is the management of the large torque (10 000 N·m per meter length of the magnet) due to the electromagnetic forces.

For the HL-LHC we consider a nested magnet with an operational field of 2.1 T, giving a magnetic length of 1.2 m and 2.1 m for each magnet type. This is achieved with Nb-Ti two-layer coils based on a Rutherford cable composed of 18 strands of 0.45 mm diameter. This cable [31] has been developed for the corresponding corrector magnet in S-LHC preparatory phase program, set up in the frame of the previous project LHC upgrade Phase I, now superseded by HL-LHC. In HL-LHC we opted for a double layer to increase the margin, and to lower the operation current below 2 kA, thus avoiding significant cost associated to the numerous (total of 24) power converters [32].

The peak field is 3.5 T, close to twice the nominal field. This is due to the presence of two perpendicular fields (giving a factor $\sqrt{2}$) plus the ratio coil peak field/bore field, which is ~1.3. Large ratios of peak field/bore field are unavoidable in dipoles where the coil width is thin with respect to the aperture. The nested option is challenging from the point of view of the mechanical structure, and to ensure reliability we require that the torque has to be controlled through a mechanical locking, see Figure 17 as proposed in [31].

The design, and construction of three prototypes (two providing 2.5 T m and one providing 4.5 T m) and 18 series magnets is an in-kind contribution of CIEMAT laboratory. The magnets are individually tested in the FREIA test station, shipped to CERN, where they are integrated in a cold mass which is then integrated in the cryostat and tested in horizontal position.

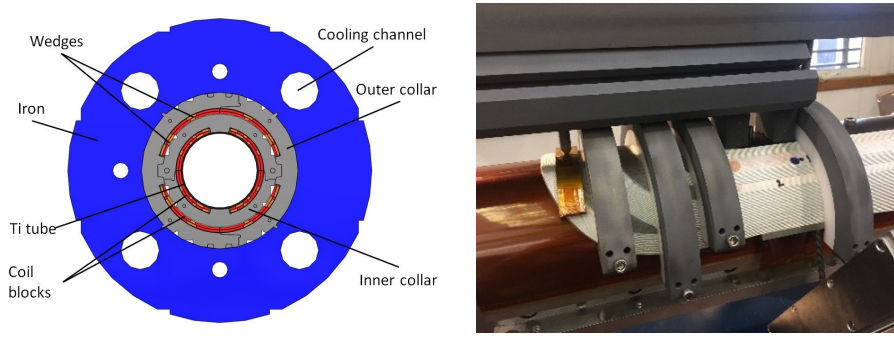

Fig. 17. Cross-section of the orbit correctors (left) and winding of the coil (right).

5.2. *Superferric correctors*

The correction of the triplet imperfections and misalignment requires a skew quadrupole, and a large set of high order correctors. The first requirement is a skew quadrupole, with 0.7 T·m integrated force, to correct the construction and alignment errors in the triplet field direction. Then we have normal and skew sextupole, octupole, decapole and dodecapole corrector magnets. Among them the sextupole is particularly relevant for the chromatic correction. Requirements for the normal and skew terms are the same, with the exception of the normal b_6 which is four times larger than a_6 since this is an allowed multipole of the quadrupole and therefore has a larger systematic and random component (see Table 2).

Table 2. Parameters of the HL-LHC correctors

Multipole	Coil Length (m)	Intehrated Gradient (T·m)	Peak Field in Coil (T)	Loadline Fraction
a2	0.457	0.700	3.6	0.44
b3/a3	0.192	0.095	2.23	0.31
b4/a4	0.172	0.069	2.09	0.31
b5/a5	0.172	0.037	1.63	0.26
b6	0.498	0.086	1.57	0.27
a6	0.123	0.017	1.50	0.27

In the LHC we have nested correctors, with up to five magnets nested. This solution saves space but makes operation more complex. For a non-nested solution, a key point is to have very short heads, otherwise all the space is lost in heads and interconnections. In the framework of the S-LHC studies, a superferric technology [31,33] was used to build some prototypes with 140 mm aperture. This solution was adopted for HL-LHC [34]: the magnets have the same cross-section as a resistive magnet (see Figures 18 and 19), with Nb-Ti coils serving to magnetize the iron poles and yoke. In this case, (i) the field quality is given by the shape of the iron poles and not by the precise location of the coils, and (ii) the field is limited at ~1.5-2 T due to iron saturation. The magnet operates at a loadline fraction between 0.25 and 0.35 (see Figure 7).

One advantage is that coils are not directly exposed to the aperture, so the magnet is resistant to radiation and additional shielding can be put to

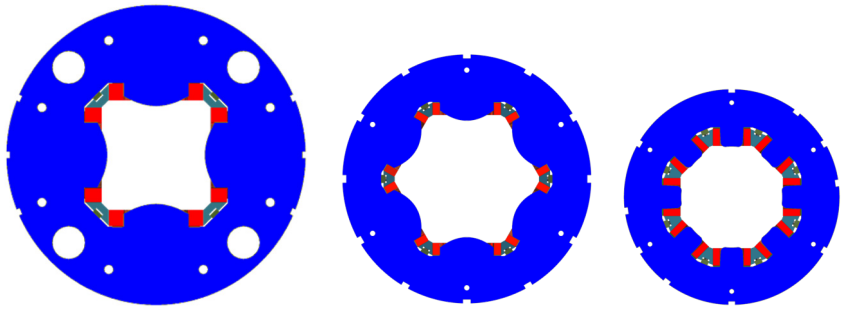

Fig. 18. Cross-section of the skew quadrupole of the sextupole and of the octupole correctors.

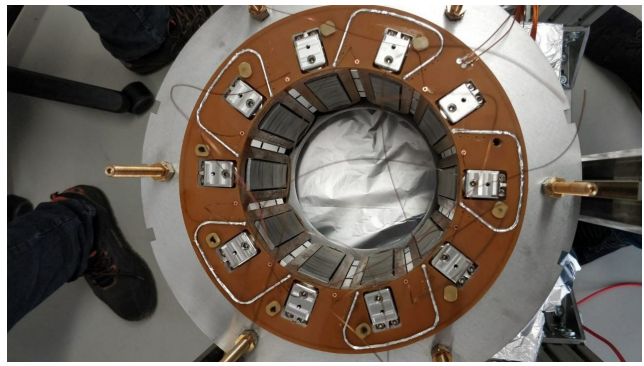

Fig. 19. Superferric decapole corrector.

protect the coils. The second advantage is that the heads can be made extremely short, with small diameter cable and sharp bends, so what is lost in the non-nested option is partially recovered by the shorter heads. It has been also checked that the longitudinal interference between different correctors is negligible even with short interconnection of 80 mm. The last advantage is that operational current is ~100 A, since the conductor is a small single wire. This also simplifies the numerous current leads needed to power this large set of correctors.

The design, and construction and test of five prototypes and 54 series magnets is an in-kind contribution of INFN-Milano-LASA. The magnets are manufactured in SAES-RIAL, tested in LASA and then shipped to CERN, where they are integrated in the cold mass with the orbit correctors or with the Q2 magnet, and then integrated in the cryostat and tested in horizontal position.

5.3. *Orbit correctors in recombination dipole*

Close to the recombination dipole two additional orbit corrector, with 5 T m integrated field in each plane, is present in the HL-LHC lattice. This corrector is absent in the LHC layout. As for the recombination dipole, the field is limited by nonlinearities in field quality induced by the cross-talk between the two apertures. Since each aperture has to work in any powering condition, the only way out is to have iron shielding between the two apertures, place the horizontal field in one aperture and the vertical in the other one to minimize the cross talk as in the LHC, and limit the operational field to 2.6 T, for a magnetic length of 2.2 m.

These requirements make this magnet ideal for the application for the titled solenoid design (also called canted cos theta or double helix in the literature). This idea first proposed in [35] and later developed in [36,37], is based on winding the conductor on grooves machined in an helix shape on an Al former. The two tilted solenoids (see Figure 20) provide a perfect dipolar field, and the opposite solenoid components cancel out. The lower efficiency of the design (some conductor is used to generate the solenoidal fields in the two concentric windings that compensate each other) is compensated by the required much simpler tooling. Moreover, for this range of field, the conductor cost is not a major component of the magnet cost.

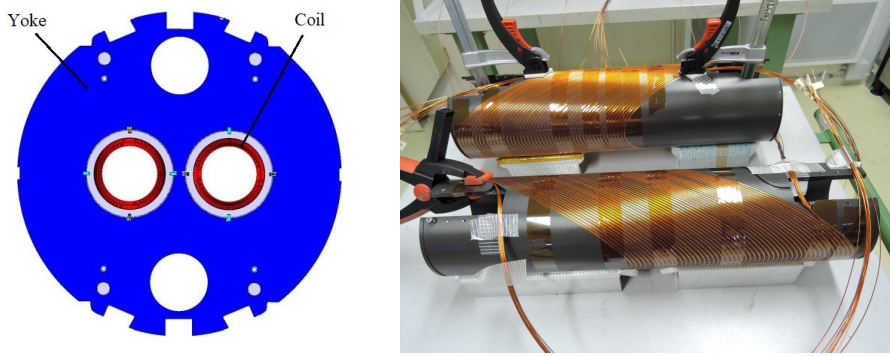

Fig. 20. Cross section of the orbit correctors in the recombination dipole (left) and its active part in a short model version: the tilted solenoid coils.

The conductor is a 0.825 mm diameter Nb-Ti strand, and 10 wires are wound in each groove. The magnet is working a 0.50 loadline fraction. The design and one prototype have been developed at CERN [38], and a technology transfer with IHEP (Beijing) has been carried out in view of an in-kind contribution by China.

A total of 14 magnets (2 prototypes, 8 series and 4 spares) are planned. Prototypes were developed in WST (Xi'an), series is ongoing in BAMA (Suzhou), with magnet test in IMP (Lanzhou). After shipping to CERN, they are integrated in the D2 cold mass, and then integrated in the cryostat and tested in horizontal position.

6. Separation Dipole

The LHC separation dipoles at IR1 and IR5 are 20-m-long resistive magnets, made of 6 modules of 3.4 m length, providing 26 T·m (see Figure 6). The new specification of integrated field in IR1 and IR5 is 35 T·m. The replacement of the resistive units with a single Nb-Ti magnet allows recovering the additional space which is needed by the longer triplet and by the insertion of crab cavities in the interaction region layout. Selecting the same aperture and the same shielding as for the triplet quadrupoles, one can verify that the collision debris induces a heat load and a radiation dose within the project targets; therefore, one can replace the resistive magnet with a superconductive one.

The main challenges in the magnet design are the large aperture giving rise to large accumulation of electromagnetic forces in the magnet midplane, fringe fields, and field quality. The large aperture gives 100 MPa pressure in the midplane due to electromagnetic forces, so a proper mechanical structure must be developed. With such a large aperture, the fringe field also becomes an issue: with a 5 T operational field in 150 mm aperture, one needs ~200 mm of iron to avoid fringe fields. In case of 15 mm coil width and 15 mm spacers, the magnet size reaches 150+(15+15+200)*2=610 in mm diameter, i.e. about the same size of the triplet quadrupole cold mass. This suggest to (i) do not push field to very large values, restricting the study to one-layer coil (ii) have a mechanical structure where forces are taken by the yoke and collars are simple spacers: in this way, more iron is available for shielding.

The baseline [14] is to set the working point at 77% of the loadline, with a Nb-Ti 15-mm-width cable as in the LHC main dipole, providing 5.6 T

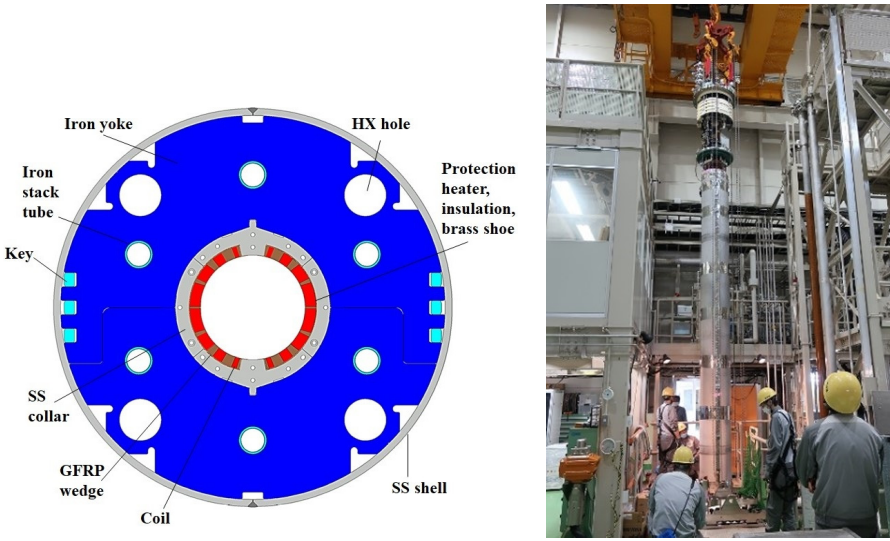

Fig. 21. Cross-section of the separation dipole (left) and prototype magnet in the test station (right).

operational field (see Figure 21). In this way a 6.3-m-long magnet provides the required 35 T·m. The iron is largely saturated at nominal field, with a 12% decrease of ratio field/current w.r.t the linear case. Such a large saturation has a relevant impact on field quality, which becomes the main challenge. A careful iron shaping can reduce this effect, following the example of what has been done for the RHIC dipoles [17]. The impact on b_3 can be reduced from the initial values of several tens of units (for a circular iron without holes) to a few units along the operational range. Optimization is done at high field, with a target for the energy reach in the window 6.5 TeV to 7 TeV.

The mechanical structure is similar to the MQXA [39], with support given by the iron yoke locked by keys. This structure has the advantage of reducing the collar size, leaving more space to iron and reducing the fringe field. It allows a very efficient collaring, providing the compression of the coil needed to avoid pole unloading during powering.

The design, construction and test of three short models, one prototype, four series and two spare magnets is an in-kind contribution of Japan via KEK laboratories. The magnet cold masses are shipped to CERN after vertical test, where they are integrated in the cryostat.

7. Recombination Dipole

The recombination dipole needs the same integrated force of 35 T·m to bring the beams back to parallel trajectories, with the nominal spacing of 192 mm. In the LHC this is done by a two-in-one 10-m-long superconducting magnet with ~3 T operational field, and 80 mm aperture. Due to the larger beam size one needs to increase this aperture to 105 mm at IR1 and IR5. In these conditions, since the beam spacing is unchanged, even with a 15-mm thin coil and 15 mm spacing for collars, only a few cm are left between the two apertures, which have the field pointing the same direction. In these conditions, the main design challenge is to decouple the magnetic field in the two apertures and ensure good field quality. For these reasons, we consider an operational field of 4.5 T (1 T lower than D1), giving a magnet length of 8 m. Even with this conservative design choice, using iron yoke as a shield between two apertures would have a limited efficiency and would lead to large saturation effects, which is difficult to compensate. Therefore, a different approach was proposed [40], following an idea proposed in [41]: the iron yoke is removed from the central part, and the resulting large but current-independent cross-talk between the apertures is corrected with a slightly (order of 1 mm) asymmetric arrangement of the conductor blocks. With this approach, it is possible to reach 4.5 T at 1.9 K with a 35% margin, and satisfying the field quality requirements.

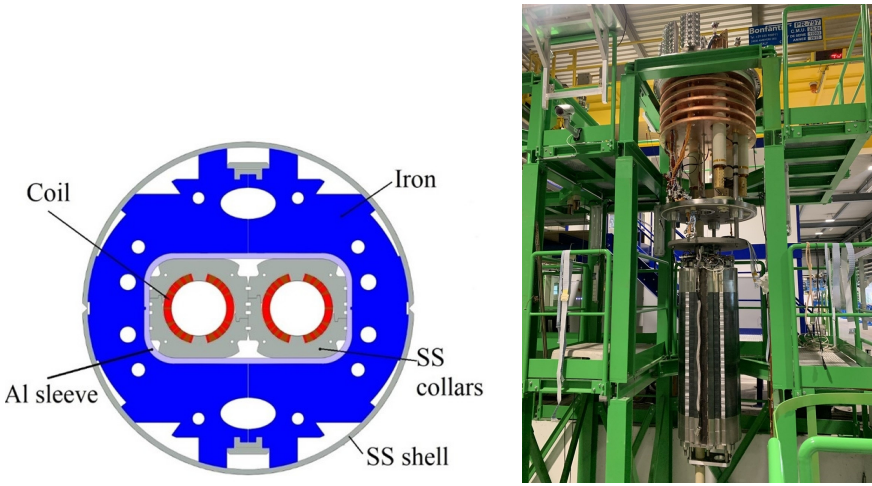

Fig. 22. Cross-section of the recombination dipole (right) and short model in the test station.

The mechanical structure (see Figure 22) relies on separate collars to increase the flexibility in manufacturing for such a small series of magnets (total of 6). The collars completely support the electromagnetic forces, and allow giving a full preload during assembly. The two apertures are assembled in a novel concept, i.e. a Al sleeve providing alignment and mechanical support to the electromagnetic forces between the two apertures (tending to separate the aperture, as the fields are in the same direction).

One short model, one prototype, four series and two spare magnets are provided an in-kind contribution by INFN-Genova, who took care of the design, with manufacture by ASG in Genova. The magnets are shipped to CERN, where they are integrated in a cold mass with the orbit correctors, and then integrated in the cryostat and tested in horizontal position.

8. The Large Aperture Two-in-one Quadrupole

In the initial layout, a larger aperture quadrupole was considered for Q4, namely increasing from the LHC values of 70 mm to 90 mm aperture. The magnet relies on a double layer Nb-Ti coil, with 120 T/m gradient, a 0.77 loadline fraction, a peak field of 6.4 T and an operating current of 4.55 kA [16]. The magnet has been removed from the baseline in 2016 after a review of the beam dynamics requirements.

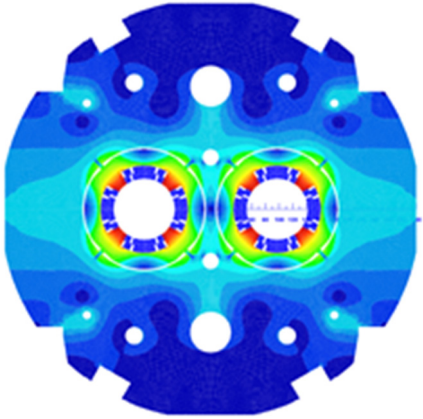

Fig. 23. Cross-section of the large aperture two-in-one quadrupole (left) and short model ready for test in CEA (right).

References

1. O. Bruning, et al., LHC luminosity upgrade: a feasibility study, *LHC Project Report* **626** (2002).
2. J. P. Koutchouk, et al., A solution for phase-one upgrade of the LHC low-beta quadrupoles based on Nb-Ti, *LHC Project Report* **1000** (2007).
3. R. Ostojic, et al., Conceptual design of the LHC interaction region upgrade: phase I, *LHC Project Report* **1163** (2008).
4. J. P. Koutchouk, Investigations of the parameter space for the LHC luminosity upgrade, *European Particle Accelerator Conference* (2006) 556-558.
5. L. Rossi, State of the art superconducting accelerator magnets, *IEEE Trans. Appl. Supercond.* **12** (2002) 219-227.
6. L. Rossi, E. Todesco, Electromagnetic design of superconducting quadrupoles, *Phys. Rev. STAB* **9** (2006) 102401.
7. N. Mokhov, et al., Protecting LHC IP1/IP5 component against radiation resulting from colliding beam interactions, *LHC project report* **633** (2003).
8. V. V. Kashikhin, et al., Quench margin measurement in Nb_3Sn quadrupole magnet, *IEEE Trans. Appl. Supercond.* **19** (2009) 2454-2457.
9. L. Esposito, et al., Fluka energy deposition studies for the HL-LHC, *International Particle Accelerator Conference*, (2013) 1379-1381.
10. R. Flukiger, T. Spina, The behaviour of copper in view of radiation damage in the LHC luminosity upgrade, *CERN Yellow Report* **2013-006** (2013) 76-82.
11. A. Tollestrup, E. Todesco, The development of superconducting magnets for use in particle accelerators: from Tevatron to the LHC, *Rev. Sci. Accel. Tech.* **1** (2008) 185-210.
12. E. Todesco, et al., A first baseline for the magnets in the high luminosity LHC insertion regions, *IEEE Trans. Appl. Supercond.* **24** (2014) 4003305.
13. E. Todesco et al. Review of the HL-LHC interaction region magnets towards series production *Supercond. Sci. Technol.* **34** (2021) 054501.
14. T. Nakamoto, et al. Model magnet development of D1 beam separation dipole for the HL-LHC upgrade *IEEE Trans. Appl. Supercond.* **25** (2015) 4000505.
15. A. Den Ouden, et al., Progress in the development of an 88-mm bore 10 T Nb_3Sn dipole magnet, *IEEE Trans. Appl. Supercond.* **11** (2011) 2268-2271.
16. H. Felice, et al., Development of MQYY: a 90-mm Nb-Ti double aperture quadrupole magnet for HL-LHC *IEEE Trans. Appl. Supercond.* **28** (2018) 4500105.
17. M. Anerella, et al., The RHIC magnet system, *Nucl. Instrum. Meths.* **A 499** (2003) 280-315.
18. R. M. Scanlan and D. R. Diedtrich, Progress and plans for the U.S. HEP conductor development program *IEEE Trans. Appl. Supercond.* **13** (2003) 1536-1541.
19. S. Gourlay, et al., Magnet R&D for the US-LHC accelerator program (LARP) *IEEE Trans. Appl. Supercond.* **16** (2006) 324-327.

20. S. E. Bartlett et al., An R&D approach to the development of long Nb3Sn accelerator magnets using the bladder and key approach *IEEE Trans. Appl. Supercond.* **15** (2005) 1136-1139.
21. G. Ambrosio, et al., Test results and analysis of LQS03 third long Nb_3Sn quadrupole by LARP, *IEEE Trans. Appl. Supercond.* 23 (2013) 4002204.
22. H. Felice, et al. Design of HQ – a high field large bore Nb3Sn quadrupole magnet for LARP *IEEE Trans. Appl. Supercond.* **19** (2009) 1235-1239.
23. P. Ferracin, et al., Development of MQXF: the Nb3Sn low beta quadrupole for the Hilumi LHC, *IEEE Trans. Appl. Supercond.* **26** (2016) 4000207.
24. X. Wang, et al., Multipoles induced by interstrand coupling currents in LARP Nb_3Sn quadrupoles, *IEEE Trans. Appl. Supercond.* **24** (2014) 4002607.
25. E. Todesco, Quench limits in the next generation of magnets, CERN Yellow Report 2013-006 (2013) 10-16.
26. T. Salmi, et al., Modeling heat transfer from quench protection heaters to superconducting cables in Nb_3Sn magnets, CERN Yellow Report **2013-006** (2013) 30-37.
27. E. Ravaioli, et al., New coupling loss induced quench protection system for superconducting accelerator magnets *IEEE Trans. Appl. Supercond.* **24** (2014) 0500905.
28. E. Ravaioli, et al., Quench protection of the first 4-m-long prototype of the HL-LHC Nb3Sn quadrupole magnets *IEEE Trans. Appl. Supercond.* **29** (2019) 4701405.
29. R. Gupta, Tuning shims for high field quality in superconducting magnets, *IEEE Trans. Magn.* **32** (1996) 2069-2073.
30. S. Izquierdo Bermudez, et al., Magnetic analysis of the MQXF quadrupole for the High-Luminosity LHC *IEEE Trans. Appl. Supercond.* **29** (2019) 4901705.
31. R. Ostojic, et al., Conceptual design of the LHC interaction region upgrade: phase I, LHC Project Report **1163** (2008).
32. J. Garcia Matos, et al., Magnetic and mechanical design of the nested orbit corrector for HL-LHC *IEEE Trans. Appl. Supercond.* **26** (2016) 4102005.
33. F. Toral, et al., Development of radiation resistant superconducting corrector magnets for the LHC upgrade, *IEEE Trans. Appl. Supercond.* **23** (2013) 4101204.
34. G. Volpini, et al. Nb-Ti superferric corrector magnets for the LHC luminosity upgrade *IEEE Trans. Appl. Supercond.* **25** (2015) 4002605.
35. D. I. Meyer and R. Flasck A new configuration for a dipole magnet for use in high energy physics applications *Nucl. Instrum. Methods* **80** (1970) 339-41.
36. C. L. Goodzeit, et al., The double-helix dipole – a novel approach to accelerator magnet design *IEEE Trans. Appl. Supercond.* **13** (2003) 1365-1368.
37. S. Caspi et al., Canted cos theta magnet (CCT) a concept for high field accelerator magnets *IEEE Trans. Appl. Supercond.* **24** (2014) 4001804.
38. G. Kirby et al., Hi-Lumi LHC twin aperture orbit correctors magnet system optimisation *IEEE Trans. Appl. Supercond.* **27** (2017) 4002805.
39. Y. Ajima, et al., "The MQXA quadrupoles for the LHC low-beta insertions, *Nucl. Instrum. Meths.* **A 550** (2005) 499-513.

40. P. Fabbricatore et al, Development of a short model of the superconducting separation dipoles D2 for the High Luminosity Upgrade of the LHC *IEEE Trans. Appl. Supercond.* **28** (2018) 4000105.
41. V. Kashikin and A. Zlobin, Design study of 2-in-1 large aperture IR dipole (D2) for the LHC luminosity upgrade Particle Accelerator Conference (2007) 464-466.